Dew point and peak fuel-rod temperature signatures in pilot-scale vacuum drying

Ji Hwan Lim[a*], Seung-Hwan Yu[a], Ju-Chan Lee [a], Kyung-Wook Shin[b], Nam-Hee Lee[b]
[a]*Radwaste Transportation and Storage R&D Division, Korea Atomic Energy Research Institute, 111 Daedeok-daero 989 beon-gil, Yuseong-gu, Daejeon 34057, Republic of Korea*
[b]*SAE-AN Engineering Corporation, #910, 184 Gasan digital 2-ro, Geumcheon-gu, Seoul, 08501, Republic of Korea*
[*]*Corresponding author: jlim@kaeri.re.kr*

***Keywords :** vacuum drying, spent nuclear fuel, dry storage, decay heat, peak cladding temperature

1. Introduction

Monitoring key thermal–hygrometric indicators during SNF vacuum drying—rather than relying solely on pass/fail dryness criteria—is increasingly important for establishing defensible operating margins. In particular, real-time tracking of (i) dew point (as a direct measure of vapor-phase moisture), (ii) peak cladding temperature (as a safety-limiting thermal parameter), and (iii) internal atmosphere temperature (which governs evaporation/desorption kinetics and sensor interpretation) provides a more physics-based understanding of drying progression and end-point behavior. Traditional practice has widely employed the pressure rebound test (PRT) to infer drying completion from pressure rise after isolation; however, pressure signals alone can be non-unique and can be affected by system volume and outgassing behavior, motivating complementary measurements that directly reflect thermodynamic state variables [1,2].

Dew-point monitoring is particularly valuable because it links the measured gas condition to water vapor partial pressure and thus to the driving force for evaporation and desorption. Goode et al. demonstrated that combining dew-point trends with pressure data enables more reliable online end-point determination than PRT alone, supporting the feasibility of identifying drying completion without intermediate exposure to atmospheric conditions [2]. More advanced implementations (e.g., gas analysis by mass spectrometry calibrated against NIST-traceable dew-point instrumentation) further illustrate the emphasis on quantifying gas-phase moisture and its evolution during drying transients [3]. In parallel, temperature measurements are essential because the achievable fuel and structure temperatures under vacuum can be constrained by limited heat transfer, and the removal of strongly bound/adsorbed water is highly temperature dependent; representative findings indicate substantially improved release at elevated temperatures (e.g., ≥220 °C) compared with near ~120 °C conditions [1]. These observations highlight why peak cladding temperature and internal atmosphere temperature must be measured and interpreted together with dew point to correctly diagnose whether the process is limited by heat-up, mass transfer, or a transition from bulk evaporation to slow desorption [1,2].

Decay heat is a central driver coupling these indicators. Higher decay heat raises internal temperatures, shifts dew-point evolution, and can accelerate progression to the cliff-edge behavior—an inflection where vapor generation and exhaust flow decrease sharply after most readily removable moisture is depleted—previously identified as a useful operational signature for end-point determination [2]. Conversely, for low-decay-heat fuel, internal temperatures may remain insufficient to sustain rapid moisture release even under deep vacuum, increasing uncertainty if only pressure-based criteria are applied [1]. Therefore, systematic experiments that correlate decay heat with peak cladding temperature, internal atmosphere temperature, and dew-point trajectories are needed to establish robust, real-time monitoring metrics and to support optimized drying procedures across a wide range of fuel and canister conditions [1–7].

In this study, we focus on experimentally characterizing how decay-heat level affects the coupled evolution of dew point, peak cladding temperature, and internal atmosphere temperature during vacuum drying, with the goal of improving real-time process understanding and strengthening the technical basis for drying end-point determination.

2. Experimental Setup and Methods

This section describes the test hardware used to monitor dew point, peak cladding temperature, and internal atmosphere temperature during vacuum drying. The overall vacuum drying facility, operating procedure, and instrumentation layout are described in greater detail in Refs. [5–7].

2.1 Mock Fuel Assembly and Fuel Rods

A scaled 17ACE7 mock fuel assembly was adopted to reproduce key geometric and heat-transfer characteristics relevant to domestic and international SNF vacuum drying processes. The overall assembly length is 1,928.4 mm, and the structure was manufactured to preserve the representative thermal

response of an actual fuel assembly under vacuum drying conditions.

The scaled 17ACE7 mock fuel rods were designed to emulate the structural characteristics of spent fuel rods. Each rod has an outer diameter (OD) of 9.5 mm and an inner diameter (ID) of 8.357 mm, with a total length of 1,746.1 mm. This configuration enables repeatable investigation of temperature evolution and thermal gradients under controlled decay-heat-equivalent heating conditions. Figure 1 presents a photograph of the experimental hardware used in this study, including the stainless-steel canister and the heater-integrated 1/2-bundle mock fuel assembly installed inside the canister prior to testing.

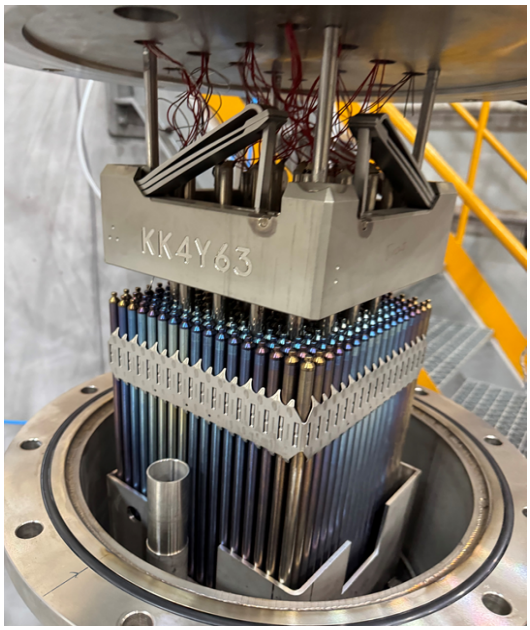

Fig. 1. Mock Fuel Assembly and Fuel Rods

2.2 Canister

The test canister was fabricated from a stainless-steel 16 in, Sch. 40 pipe. The canister has an OD of 406.4 mm, a length of 2,000 mm, and a wall thickness of 12.7 mm. The design provides mechanical robustness and stable thermal boundary conditions during vacuum drying, allowing the mock assembly to be housed securely while limiting distortion and external heat loss.

The lid flange was manufactured with an OD of 466.4 mm and a thickness of 30 mm, and the bottom plate was also designed with an OD of 406.4 mm and a thickness of 30 mm. These dimensions were selected to ensure structural integrity and to support reliable internal temperature and pressure conditions during elevated-temperature operations.

2.3 Electric Heaters and Fabrication Specifications

Electric heaters serve as the primary heat source of the system and were fabricated from stainless steel for durability and high-temperature corrosion resistance. Each heater has an OD of 9.6 mm and is installed inside the guide tube of the 17ACE7 mock assembly (guide tube ID: 10 mm) to ensure proper fit and alignment.

The heated (active) length of each heater is 1,614 mm. The heater installation was configured to promote a stable axial heat distribution: the distance from the lid reference is 1,914 mm, and the distance from the bottom is 91 mm (calculated as 60.53 + 25.41 + 5). A total of 24 heaters were installed, and each heater can be controlled independently to enable flexible power shaping and uniform heating as required by the test matrix.

2.4 Controller and Electrical Control System

Heater power was controlled within 0–150 W per channel using a voltage-control scheme with a 1 V adjustment resolution. A dedicated control panel enabling 24 independent voltage channels was used to operate and tune each heater individually.

Voltage and current were monitored in real time using D/P panel meters, allowing stable operation and rapid identification of abnormal electrical behavior. This multi-channel control architecture supports repeatable thermal boundary conditions and minimizes uncertainty in interpreting measured dew-point and temperature signals during drying transients.

2.5 Lid and Feed-through Configuration

The canister lid was fabricated from stainless steel with a diameter of 520 mm and a thickness of 35 mm. A 5 mm clearance was maintained between the lid inner surface and the canister cavity interface to reduce mechanical interference and mitigate heat-loss pathways during thermal cycling.

To install the heater power lines and temperature-instrumentation wiring, the lid includes 31 feed-through ports: 24 dedicated to the electric heaters and 7 allocated for thermocouple signal lines attached to the mock fuel rods. The feed-through layout was designed to be consistent with the relative positions of the mock rods and guide tubes, enabling organized routing and minimizing measurement interference. Additional details of the vacuum drying experimental facility, including system integration and test operation, are available in Refs. [5–7].

3. Experimental Results

3.1. Vacuum Drying Procedure

Figure 2 compares the canister pressure histories obtained with the conventional method (step-wise) and the mechanism-based vacuum drying approach. In the

conventional method, the pressure evolution is characterized by repeated pump-down and hold segments, which create intermittent stagnation periods in the canister. These interruptions tend to maintain a warm and moisture-rich internal environment for an extended duration. In contrast, the mechanism-based vacuum drying approach modulates pumping to intentionally maintain residence in a targeted transitional pressure range (around several tens of Torr), while still allowing continuous discharge pathways. This operational difference is important because it conditions how vapor is continuously removed and how the internal thermodynamic state evolves during pressure reduction, which is reflected in the dew-point and temperature behaviors discussed in the following subsections.

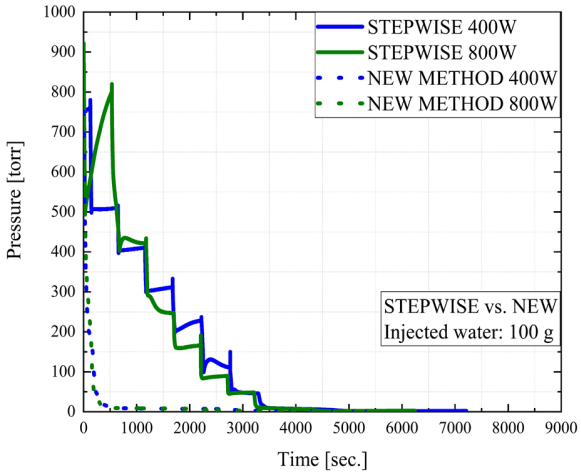

Fig. 2. Time evolution of canister pressure: comparison between the conventional method (step-wise) and mechanism-based vacuum drying.

3.2. Dew Point Analysis

Figure 3 shows the dew-point response as a function of decreasing pressure for both methods. With the conventional method, the dew point remains nearly constant at approximately 22–24 °C over a broad pressure range (e.g., from ~800 Torr down to ~50 Torr), with only brief downward spikes during step transitions; the signal then exhibits a sharp cliff-like drop near the late stage, passing through 0 °C and reaching approximately −20 °C (or slightly below) within a short time interval. This behavior indicates that the canister atmosphere stays close to saturation for most of the process and transitions to a dry state abruptly only near the end.

By contrast, the mechanism-based vacuum drying approach exhibits a fundamentally different trajectory: the dew point decreases gradually from the beginning (e.g., 22 °C → 10 °C → 0 °C → −10 °C), and at around 20–40 Torr it drops more steeply into the negative range. The context explains that this pressure band is critical because (i) capillary thresholds in narrow gaps can release sequentially near this region, and (ii) the gas-flow regime becomes favorable for purging non-condensable gas trapped in crevices while sustaining a pressure differential that supports continuous discharge. As a result, in the mechanism-based approach the reduction in total pressure is accompanied by a concurrent reduction in water vapor partial pressure, producing a clear and interpretable dew-point decline throughout pump-down rather than a late-stage collapse.

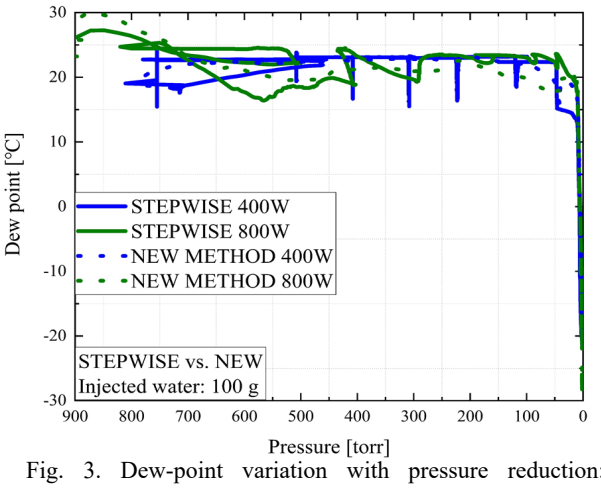

Fig. 3. Dew-point variation with pressure reduction: comparison between the conventional method (step-wise) and mechanism-based vacuum drying.

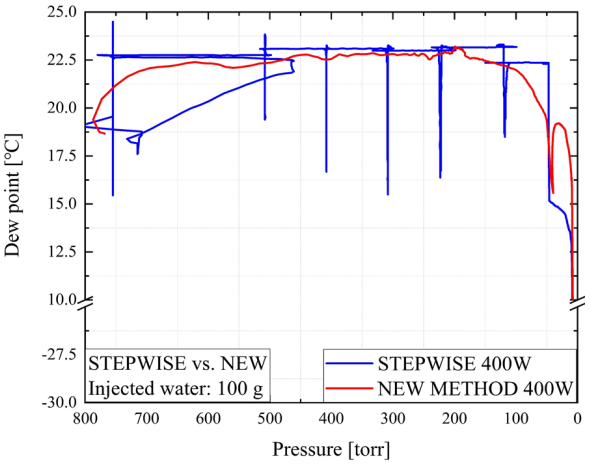

Fig. 4. Expanded view near the pre-drop region: precursor dome behavior in dew point prior to the sharp decrease.

Figure 4 magnifies the behavior immediately prior to the dew-point cliff. In the conventional method, the canister dew point stays nearly flat (≈22–23 °C) with little precursor signal, aside from narrow dips associated with step switching. In contrast, the mechanism-based approach shows a small but distinct dome feature: the dew point initially rises slightly (from ~19–20 °C to ~22–23 °C around ~250 Torr) and then begins to decline gradually into single-digit °C values as pressure drops below ~100 Torr. The document interprets this dome as a physically meaningful precursor: immediately before the sharp decline,

evaporation from internal gaps temporarily increases vapor concentration, followed by progressive threshold release and rapid vapor depletion. Practically, the onset of the post-dome downward slope can be treated as an early warning that a rapid dew-point drop—and thus a drying end-point signature—is imminent, whereas such early predictability is limited when using the conventional method.

3.3. Internal Atmosphere Temperature

Figure 5 presents the time evolution of internal canister atmosphere temperature measured under the mechanism-based vacuum drying approach. The temperature trend provides an additional process-state indicator that complements dew point, because it reflects the coupled effects of heat input, vapor generation, and gas replacement during pump-down. Under mechanism-based control, the temperature evolution can be interpreted together with the sustained operation in the transitional pressure range: as vapor is continuously discharged and the internal atmosphere becomes progressively drier, the internal thermal response becomes more stable and interpretable as a process trajectory rather than a sequence of stepwise disturbances.

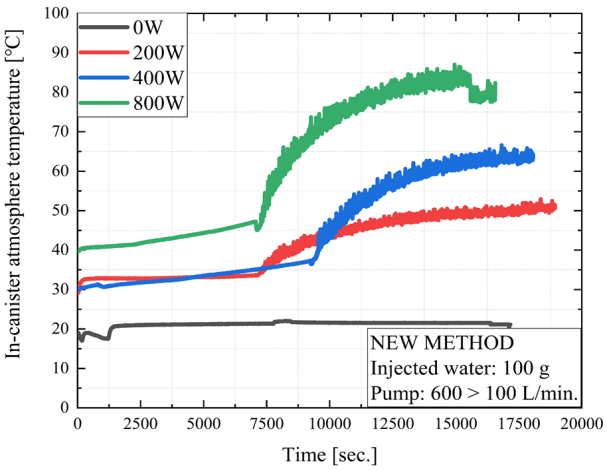

Fig. 5. Time evolution of internal canister atmosphere temperature under mechanism-based vacuum drying.

3.4. Fuel-Rod Surface Temperature

Figure 6 compares the fuel-rod surface temperature response versus pressure for the conventional method (step-wise) and the mechanism-based vacuum drying approach. The results indicate that the mechanism-based approach enables the system to spend a longer period in a higher-temperature regime (approximately 170–200 °C in the high-power case described), while simultaneously maintaining a drier atmosphere. The document emphasizes that this combination is significant because the 170–200 °C range is associated not only with removal of liquid films and weakly adsorbed water but also with dehydration/dehydroxylation of hydroxylated surface species (–OH), which can release additional moisture that would otherwise be prone to reattachment under near-saturated conditions. Accordingly, when the mechanism-based approach passes through this regime under dry-gas conditions, released moisture is more effectively swept out, whereas under the conventional method the atmosphere remains closer to saturation and repeated wetting/reattachment can persist during holds.

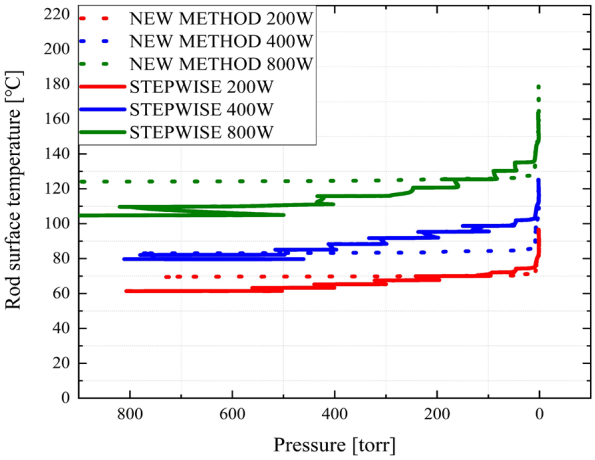

Fig. 6. Fuel-rod surface temperature variation with pressure reduction: comparison between the conventional method (step-wise) and mechanism-based vacuum drying.

4. Conclusions

This study compared a conventional method (step-wise) vacuum drying procedure with a mechanism-based vacuum drying approach using canister pressure, dew point, internal atmosphere temperature, and fuel-rod surface temperature signals. The results show that the conventional method maintains a near-saturated canister atmosphere (dew point ≈ 20–24 °C) through much of the pump-down, followed by an abrupt late-stage cliff drop to sub-zero dew points, providing limited precursor information for end-point anticipation. In contrast, the mechanism-based approach produces a gradual dew-point decline from the early stage and a pronounced pressure-dependent transition near the 20–40 Torr region, consistent with sustained vapor removal and sequential release of capillary thresholds, thereby yielding a more interpretable and predictive drying trajectory. A notable pre-drop dome feature observed only in the mechanism-based approach provides an actionable precursor signature that can support earlier and more reliable end-point recognition compared with the conventional method. Finally, the mechanism-based approach enables prolonged operation in a high surface-temperature regime (~170–200 °C) under dry-atmosphere conditions, which is important for preventing reattachment of released moisture and for promoting dehydration/dehydroxylation-related moisture removal, whereas the conventional method is more prone to maintaining saturated conditions during holds that can

facilitate repeated wetting and reattachment. Overall, the combined pressure–dew point–temperature evidence supports that mechanism-based vacuum drying improves process observability and strengthens the technical basis for identifying drying completion.

Acknowledgements

This work was supported by the Institute for Korea Spent Nuclear Fuel (iKSNF) and National Research Foundation of Korea (NRF) grant funded by the Korea government (Ministry of Science and ICT, MSIT) (No. 2021M2E1A1085226).

REFERENCES

[1] d'Entremont, A., Smith, R., Rirschl, C., Waldrop, K., Dunn, D., Einziger, R., & Sindelar, R. (2024). Drying of Spent Nuclear Fuel: Considerations and Examples. Nuclear Technology, 210(9), 1639–1647.

[2] Goode, J. B., Hambley, D. I., & Hanson, B. C. (2019). End point determination for spent nuclear fuel drying operations. Progress in Nuclear Energy, 116, 108–114.

[3] Pulido, R. J., Taconi, A. M., Williams, R. W., Baigas, B. T., & Durbin, S. G. (2024). Quantification of Residual Water in Spent Fuel Dry Storage Canisters Using Mass Spectrometry (No. SAND-2024-03859R). Sandia National Laboratories.

[4] Saha, S., Khan, J., Knight, T., & Farouk, T. (2022). A global model for predicting vacuum drying of used nuclear fuel assemblies. Nuclear Technology, 208(3), 414–427.

[5] Lim, J. H. (2026). A critical review of spent nuclear fuel drying. Progress in Nuclear Energy, 193, 106196.

[6] Lim, J. H., Yu, S. H., Chae, G. S., Shin, K. W., & Lee, N. H. (2026). How much residual water remains in a canister after vacuum drying for spent nuclear fuel storage?. Progress in Nuclear Energy, 193, 106231.

[7] Lim, J. H., Bang, K. S., Yu, S. H., Shin, K. W., Lee, N. H., & Chae, G. S. (2025). Improving spent nuclear fuel vacuum drying efficiency via pump modulation at the liquid–vapor phase transition. Applied Thermal Engineering, 128628.